

Quantitative prediction of ischemic stroke tissue fate

Qiang Shen and Timothy Q. Duong*

Departments of Neurology and Radiology, Neuroscience Division, Yerkes Imaging Center, Emory University, Atlanta, GA, USA

Received 8 January 2008; Revised 7 February 2008; Accepted 7 February 2008

ABSTRACT: Accurate prediction of ischemic tissue fate could aid clinical decision-making in the treatment of acute stroke. We investigated predictions of tissue fate for three (30-min, 60-min and permanent) stroke models in rats. Quantitative cerebral blood flow (CBF), apparent diffusion coefficient (ADC) and spin–spin relaxation time constant (T_2) were acquired during the acute phase and at the end point followed by histological examination. Probability-of-infarct profiles based on ADC and CBF data were constructed using a training dataset. Probability-of-infarct maps were predicted using only acute stroke data from a separate experimental dataset, revealing the likelihood of future infarction. Performance measures of sensitivity and specificity showed accurate predictions. Sensitivities (mean \pm SD) for the 30-min, 60-min and permanent stroke were, respectively, $82 \pm 6\%$, $82 \pm 7\%$, and $86 \pm 4\%$, specificities were $83 \pm 5\%$, $86 \pm 5\%$, and $89 \pm 6\%$, and the areas under the receiver operating curve were $87 \pm 3\%$, $90 \pm 4\%$, and $93 \pm 3\%$. Importantly, to improve prediction accuracy, we took into account regional susceptibility to infarction. Spatial frequency-of-infarct maps were constructed and predictions were made by taking the weighted average of the probability-of-infarct map and spatial frequency-of-infarct map. The optimal weighting coefficient of spatial frequency-of-infarct was small (10%) for the permanent occlusion group but surprisingly large (40%) for the reperfusion groups, indicating that regional susceptibility of infarction was important for accurate prediction in reperfusion stroke. We concluded that the likelihood of cerebral infarction in rats can be accurately predicted and that accounting for regional susceptibility of infarct further improves prediction accuracy. Predictive models have the potential to provide a valuable quantitative framework for clinicians to consider different stroke treatment options. Copyright © 2008 John Wiley & Sons, Ltd.

KEYWORDS: predictive model; ischemic penumbra; perfusion–diffusion mismatch; diffusion-weighted imaging; perfusion-weighted imaging

INTRODUCTION

Ischemic stroke occurs when basal cerebral blood flow (CBF) falls below a critical threshold (1–4), resulting in energy failure, which is subsequently manifested as a reduction in the apparent diffusion coefficient (ADC) of water (5). Perfusion-weighted and diffusion-weighted MRI is very sensitive to acute stroke changes and is becoming the method of choice for diagnosing and characterizing acute ischemic brain injury. During early ischemic injury, a central core of severely compromised CBF and severe ADC reduction is typically surrounded by tissue with moderately diminished CBF, near-normal ADC, and impaired electrical activity, but preserved cellular metabolism. Although the mechanism of ADC

reduction remains poorly understood, the difference in anatomical area defined by perfusion-weighted and diffusion-weighted images, commonly referred to as the ‘perfusion–diffusion’ mismatch (6,7), approximates the potentially salvageable ‘ischemic penumbra’ (1–4) and thus has important practical and clinical utility.

One implication of the above observations is that diffusion and perfusion MRI data on acute stroke can be used to statistically predict the final ischemic tissue fates in different brain structures. The ability to do so could aid clinical decision-making in the treatment of acute ischemic brain injury (8). *Ad hoc* predictions made during an acute stroke phase on the basis of ADC and CBF critical thresholds have been correlated with end-point imaging and stroke outcomes (9,10). Statistical prediction based on acute stroke data with correlation via histology and end-point imaging has been demonstrated in rats and humans (11–13). The ischemic penumbra is remarkably heterogeneous (14,15). Although ADC and CBF are strong predictors of tissue infarction following acute stroke, some brain regions are more susceptible to infarct than others. Factors that contribute to regional susceptibility to ischemic injury include distance from patent afferent vessels, basal regional blood flow, and metabolism. For example, tissues close to the anterior

*Correspondence to: T. Q. Duong, Yerkes Imaging Center, Emory University, 954 Gatewood Road NE, Atlanta, GA 30329, USA.
E-mail: tduong@emory.edu

Contract/grant sponsor: NIH; contract/grant number: R01-NS45879.
Contract/grant sponsor: American Heart Association; contract/grant number: SDG-0430020N and SDG-0830293N.

Abbreviations used: ADC, apparent diffusion coefficient; CBF, cerebral blood flow; ISODATA, iterative self-organizing data-analysis algorithm; P_I , probability-of-infarct; P_D , probability-of-infarct density; MCAO, middle cerebral artery occlusion; ROC, receiver operating characteristic.

communicating artery and the posterior cerebral artery have lower infarct incidences because of sustained or partial collateral flow (16). Conversely, the hippocampus is more susceptible to ischemic injury (17). Thus, using information on regional susceptibility to ischemic injury to predict tissue fate has the potential to improve its accuracy.

The goals of this study were: (i) to develop and apply a prediction algorithm to carefully document the probability profiles and probability-of-infarct density profiles for three representative (30-min, 60-min, and permanent) intraluminal middle cerebral artery occlusion (MCAO) durations in a rat stroke model; (ii) to predict the final ischemic tissue fate using only acute stroke data, validate it using histology, and quantify prediction accuracy using performance measures; (iii) to predict tissue fates in animals with the hypothetical scenario of no reperfusion in the reperfusion groups; (iv) to improve prediction accuracy by accounting for regional susceptibility to ischemic injury. Quantitative perfusion, diffusion, and T_2 image data were acquired every 30 min during the acute phase up to 180 min after ischemia, and again at 24 h followed by histological examination. Different tissue types (normal, mismatch, and ischemic core) were classified by using the improved iterative self-organizing data-analysis algorithm (ISODATA) clustering method (16), as opposed to a threshold-based analysis. Pixel-by-pixel predictions were evaluated, revealing different likelihoods of infarct in different tissue types. An accurate predictive approach should help to individualize treatment windows and potentially extend current treatment window options.

METHODS

Animal preparations

Three different occlusion durations were studied: 30-min MCAO ($n = 12$), 60-min MCAO ($n = 12$), and permanent MCAO ($n = 12$). Stroke surgery and animal preparations have been described elsewhere (18–20). For each occlusion group, half of the animals were randomly assigned to the training group for generation of probability profiles; predictions were made on the remaining half, the experimental group. End-point imaging was performed at 24 h followed by histological examination with 2,3,5-triphenyltetrazolium chloride. Histological infarct volume was determined with edema correction (20).

Sprague–Dawley rats (300–350 g) were initially anesthetized with chloral hydrate (400 mg/kg, intraperitoneal injection) and subjected to intraluminal MCAO. A femoral artery was catheterized for blood gas sampling and continuous blood pressure and heart rate monitoring. Blood pressure, heart rate, respiration rate, rectal temperature, and blood gases were maintained within

normal physiological ranges. Once the animal was in the magnet, $\sim 1\%$ isoflurane was used. The animals breathed spontaneously without mechanical ventilation (20,21).

MR experiments

MRI was performed on a Bruker 4.7 T/40 cm scanner (Bruker, Billerica, MA, USA). The animal was secured in a stereotaxic headset and placed on an animal holder, consisting of a surface coil (2.3 cm internal diameter) for brain imaging and a butterfly neck coil for arterial spin labeling (20). Coil-to-coil interaction was actively decoupled. Imaging was performed at 30, 60, 90, 120, and 180 min, and again at ~ 24 h after occlusion.

ADC maps were obtained by averaging three ADC datasets acquired with diffusion-sensitive gradients applied along the x , y , or z direction. Data were acquired using spin-echo echo-planar imaging [matrix = 128×128 (four shot for permanent MCAO) or 64×64 (single shot for 30-min and 60-min MCAO), field of view = $2.56 \text{ cm} \times 2.56 \text{ cm}$, $TR = 2 \text{ s}$ per segment (90° flip angle), $TE = 37.5 \text{ ms}$, $b = 10$ and 1270 s/mm^2 , $\Delta = 17.53 \text{ ms}$, $\delta = 5.6 \text{ ms}$, seven 1.5 mm slices, and 16 averages]. Higher resolution in the permanent MCAO was a result of our recent successful attempt to achieve better ischemic definition. Higher resolution should improve prediction by reducing partial-volume effects, but it has lower signal-to-noise ratio per unit time, which could increase the uncertainty of the prediction results. However, differences in resolution of the data here are not expected to alter the overall conclusion of the prediction results.

Quantitative CBF was measured using the continuous arterial spin-labeling technique (22) with gradient-echo echo-planar imaging and parameters similar to the ADC measurement except $TE = 20 \text{ ms}$. Paired images were acquired alternately – one with and the other without arterial spin-labeling preparation. Seventy-six pairs of images were acquired for signal averaging, with half acquired before and the other half after the ADC measurements.

T_2 -weighted images were acquired 24 h after occlusion using the fast spin-echo pulse sequence (TE per echo = 6.5 ms) with two different effective TE s (52 and 104 ms), echo train length 16, and 16 signal averages.

Data analysis

Data analyses used codes written in Matlab (MathWorks, Natick, MA, USA) and STIMULATE software (University of Minnesota). Six anterior slices were analyzed to avoid susceptibility distortion around the ear canals. Images were co-registered between acute phase and 24 h data within the same animals as well as between animals using custom-designed semi-automatic co-registration software. This approach has been used successfully (21,23,24).

Data were reported as mean \pm SD, with $P < 0.05$ (t -test) taken to be statistically significant.

ADC and CBF calculation. ADC maps with intensity in units of mm^2/s were calculated pixel-by-pixel (20,21). CBF maps (S_{CBF}) with intensity in units of $\text{mL}/\text{g}/\text{min}$ were calculated (22) pixel-by-pixel using $S_{\text{CBF}} = \lambda/T_1(S_C - S_L)/[S_L + (2\alpha - 1)S_C]$, where S_C and S_L are signal intensities of the unlabeled and labeled images, respectively. λ , the water brain–blood partition coefficient, was taken to be 0.9 (25). T_1 , the water spin-lattice relaxation time of tissue, was measured to be 1.5 s at 4.7 T. α , the arterial spin-labeling efficiency (26), was measured to be 0.8. The continuous arterial spin labeling technique used here has some limitations (27). Acute ischemia has been reported to change tissue T_1 up to 6–20% (28–31), and our CBF model which assumes a constant normal T_1 could overestimate CBF by the same magnitude in the ischemic regions. The CBF model used here also ignores transit time and permeability effects, which could change significantly in stroke (27). Improving the accuracy of quantitative blood-flow MRI especially under perturbed conditions remains an active area of research.

ISODATA cluster analysis of lesion volumes. ISODATA (32) is an effective clustering method. Unlike many other existing techniques, ISODATA analysis requires minimal user intervention and the number of clusters is statistically determined (33,34). ISODATA analysis was improved with Mahalanobis measure and spatial contiguity (16). Pixels of cerebrospinal fluid and the corpus callosum were first excluded using ISODATA. ISODATA was then used to identify pixels belonging to different tissue zones based on ADC and CBF data, and to determine the final lesion volume based on end-point MRI data. Multiple clusters were statistically resolved and identified as ‘normal’, ‘mismatch’, and ‘ischemic core’ from the ischemic right hemisphere. The ischemic core was determined using ADC, CBF and T_2 maps 24 h after occlusion.

Probability profiles and probability-of-infarct (P_I) maps. Using the training group, profiles of the P_I contour plots were derived as a function of ADC versus CBF by determining the percentage of pixels within each grid that had migrated to the ischemic core 24 h after ischemia. Grid sizes of $0.05 \times 10^{-3} \text{ mm}^2/\text{s}$ for ADC and $0.1 \text{ mL}/\text{g}/\text{min}$ for CBF were used. P_I contour plots were displayed with color coding ranging from 0% to 100% in steps of 10%. This constituted the look-up table basis sets for use of prediction. Normalized probability of infarct density (P_D) contour plots at different time points after ischemia were also computed by multiplying the P_I by the number of pixels in each grid. P_D was normalized within each occlusion group, allowing comparison of relative density among different tissue zones.

Predictions of subsequent infarction were made on the experimental group using only the 30-min (or 60-min for the 60-min MCAO group) data by looking up the corresponding P_I contour plots of the training group on a pixel-by-pixel basis. A 3×3 Hanning filter was used to smooth the P_I maps. Acute ADC and CBF data (30 min or 60 min after ischemia) were used in the prediction because they were informative during the acute phase (5), whereas T_2 did not change until a few hours after occlusion, coinciding with the advent of vasogenic edema.

Performance measures of the prediction. Sensitivity, specificity, receiver operating characteristic (ROC) curves and optimal operating point were computed to evaluate prediction performance. The number of pixels predicted to infarct that actually did infarct [true positives (TP)], the number of pixels that did not infarct [false positives (FP)], the number of pixels predicted not to infarct that remained non-infarcted [true negatives (TN)] and those that became infarcted [false negatives (FN)] were determined. Sensitivity, defined as the true positive ratio $\text{TPR} = \text{TP}/(\text{TP} + \text{FN})$, and specificity, defined as the true negative ratio $\text{TNR} = \text{TN}/(\text{TN} + \text{FP})$, were calculated. ROC curves and the optimal operating point were derived (16).

Spatial frequency-of-infarct. To improve prediction accuracy, we took into account the regional susceptibility to ischemic injury. Spatial frequency-of-infarction maps were obtained by counting the frequency of infarction across animals. Images from different animals within the same MCAO group were spatially co-registered, and the frequency-of-infarct maps were computed pixel by pixel using the following equation

$$\begin{aligned} & \text{Spatial frequency of infarct}(x, y, z) \\ &= \frac{\text{Number of animals of pixel}(x, y, z)\text{infarcted}}{\text{Total number of animals}} \end{aligned}$$

where x ranged from 1 to 64 or 128, y ranged from 1 to 64 or 128, and z ranged from 1 to 6.

Predictions were made by taking the weighted average of the P_I map and the frequency-of-infarct map. ROC analysis was performed to determine the optimal weighting coefficients. For the regional susceptibility weighting coefficient from 0.1 to 1 in steps of 0.1, the areas under the ROC curves obtained from the ROC analysis of the predicted tissue fate against the end-point imaging data were evaluated. The areas under the ROC curves were plotted as a function of the regional susceptibility weighting coefficients, and the peaks of these ROC curves were selected as the optimal. Results from histological examination and predictions made with and without regional susceptibility information were compared.

RESULTS

Probability-of-infarct (P_1)

Two-dimensional P_1 contour profiles of ADC and CBF values for the 30-min, 60-min and permanent MCAO at various time points after ischemia are shown in Fig. 1 (training dataset, $n = 6$). For the purpose of discussion only, the 'normal' zone is considered as $ADC > 0.53 \times 10^{-3} \text{ mm}^2/\text{s}$ and $CBF > 0.3 \text{ mL/g/min}$, the 'core' zone as ADC below these values, and the 'mismatch' zone as $CBF < 0.3 \text{ mL/g/min}$, but $ADC > 0.53 \times 10^{-3} \text{ mm}^2/\text{s}$ (20). Actual tissue classifications used ISODATA clustering.

Before reperfusion, P_1 increased with decreasing ADC and CBF. P_1 in the core zone of the 30-min and 60-min MCAO was lower than for the permanent MCAO, and the P_1 in the mismatch zone was essentially zero for the

30-min MCAO. These results indicate that: (i) different occlusion groups showed different likelihoods of infarction in different tissue zones; (ii) most of the mismatch pixels in the permanent MCAO were destined to infarct; (iii) some mismatch pixels in the 60-min MCAO were destined to infarct; (iv) only a few mismatch pixels in the 30-min MCAO were destined to infarct.

After reperfusion, P_1 increased in all tissue zones, suggesting that a substantial amount of tissues showed at least transient CBF and ADC recovery, although some of these tissues subsequently became infarcted. CBF in most of the tissue changed to normal or close to normal immediately after reperfusion. In the 30-min MCAO, most of the initially recovered pixels that migrated to the normal zone showed low P_1 , in marked contrast with the 60-min MCAO where many of the initially recovered tissues did subsequently become infarcted. One explanation is that longer occlusion durations trigger delayed

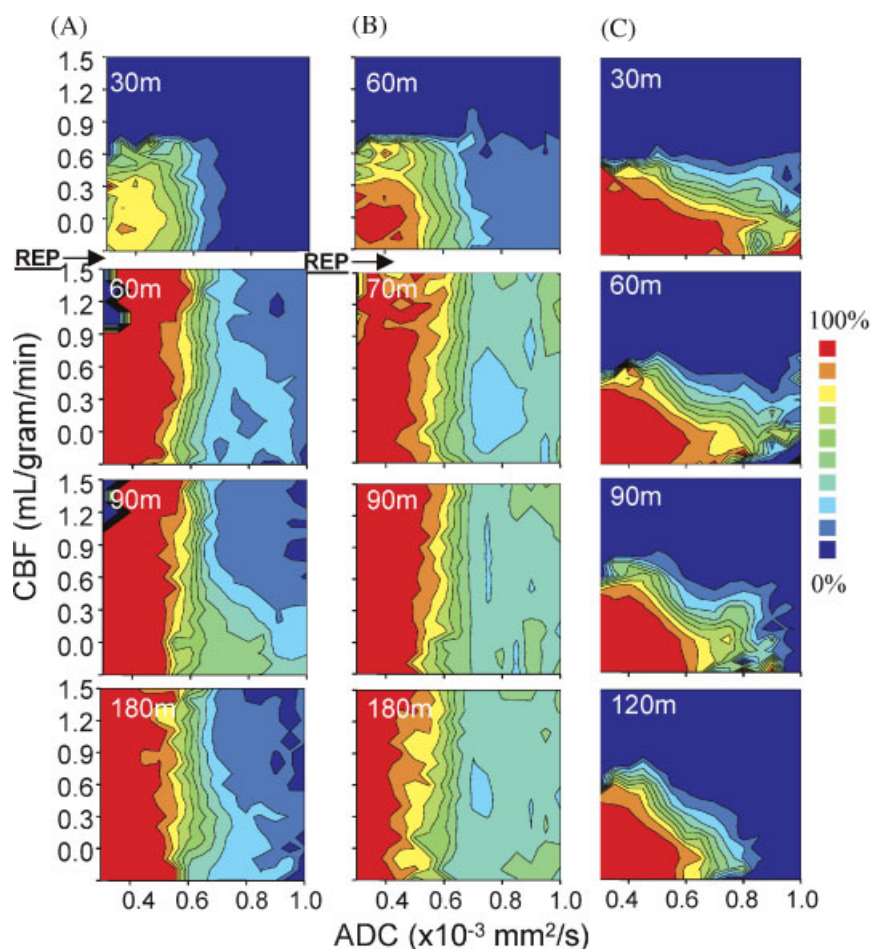


Figure 1. Profiles of probability-of-infarct (P_1). P_1 of CBF versus ADC at different time points after ischemia for three different occlusion durations: (A) 30-min MCAO ($n = 6$), (B) 60-min MCAO ($n = 6$) and (C) permanent MCAO ($n = 6$). 'Rep' indicates the time point when reperfusion took place. The 120-min time points for 30-min and 60-min MCAO are not shown. These data are from the training groups. The blue–red color bar indicates the probability ranging from 0% to 100%. Note that there are a few pixels (1–2%) with slightly negative CBF values, which were due to 'noise' for pixels with close to zero blood flow. This figure is available in colour online at www.interscience.wiley.com/journal/nbm

infarction. In the 30-min and 60-min MCAO group, the tissue zone with low ADC and high CBF also showed significant P_I because this region represented mostly dead/injured tissue with high blood flow after reperfusion.

Probability-of-infarct density (P_D)

A P_D contour plot is a product of the P_I within a grid and the number of infarcted pixels belonging to that grid (Fig. 2, training dataset). Before reperfusion, P_D distributions were highly localized to the core zone. After reperfusion, P_D became less 'localized' as expected. By the 90-min time point and onward, P_D contour plots showed two peaks in the 30-min and 60-min MCAO groups but only one peak in the permanent MCAO group. In the 30-min MCAO group, most of the initially recovered tissues that migrated to the normal zone did not become infarcted and, furthermore, most of the tissues that subsequently became infarcted came from the

mismatch and core zones. In contrast, in the 60-min MCAO group, many of the initially recovered tissues that migrated to the normal zone did become infarcted, and most of the tissue that subsequently became infarcted came from all three tissue zones. At the 180-min time point, the 30-min MCAO group still showed high P_D in the mismatch and normal zones, suggesting that the tissue fate was still evolving compared with the 60-min and permanent MCAO groups.

P_I prediction maps

Pixel-by-pixel risk predictions of subsequent infarction were computed on separate groups of animals based only on acute CBF and ADC data acquired at the representative time point of 30 min after ischemia (Fig. 3, experimental dataset, $n = 6$). The predicted infarct maps showed excellent pixel-by-pixel correspondence to ISODATA cluster analysis of the end-point MRI data

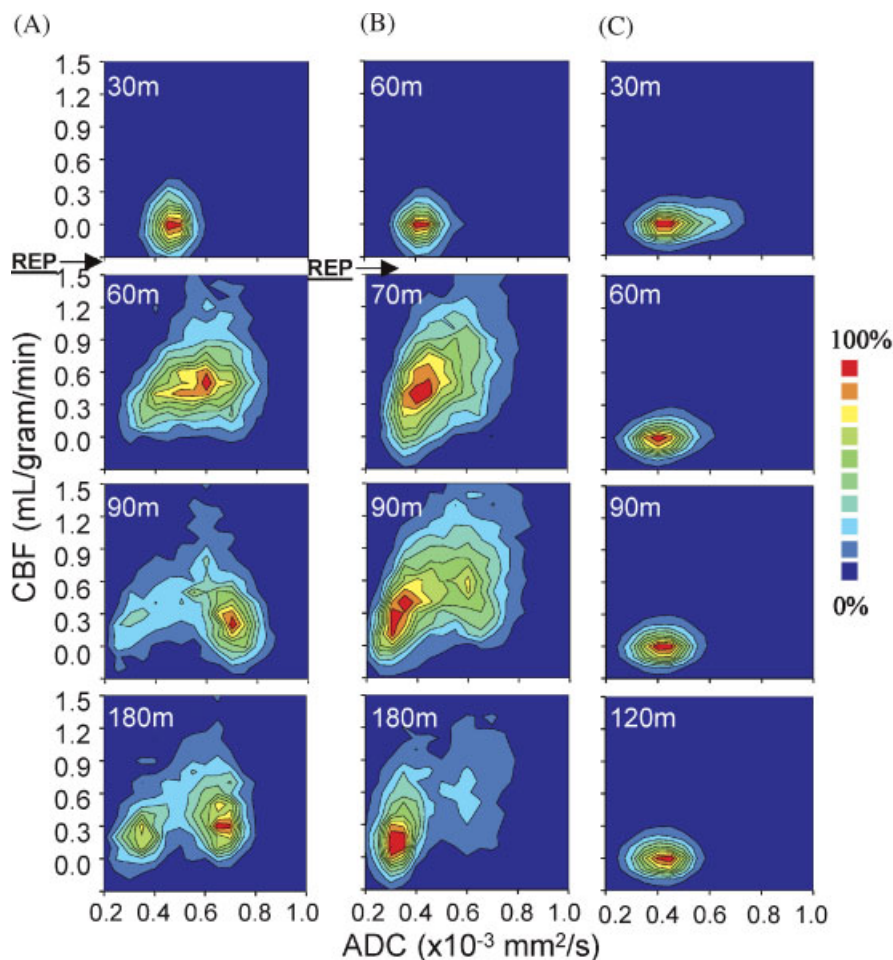


Figure 2. Profiles of probability-of-infarct density (P_D). P_D of CBF versus ADC at different time points for three different occlusion durations: (A) 30-min MCAO ($n = 6$), (B) 60-min MCAO ($n = 6$) and (C) permanent MCAO ($n = 6$). These data are from the training groups. Probability density profiles were normalized from 0% to 100%. This figure is available in colour online at www.interscience.wiley.com/journal/nbm

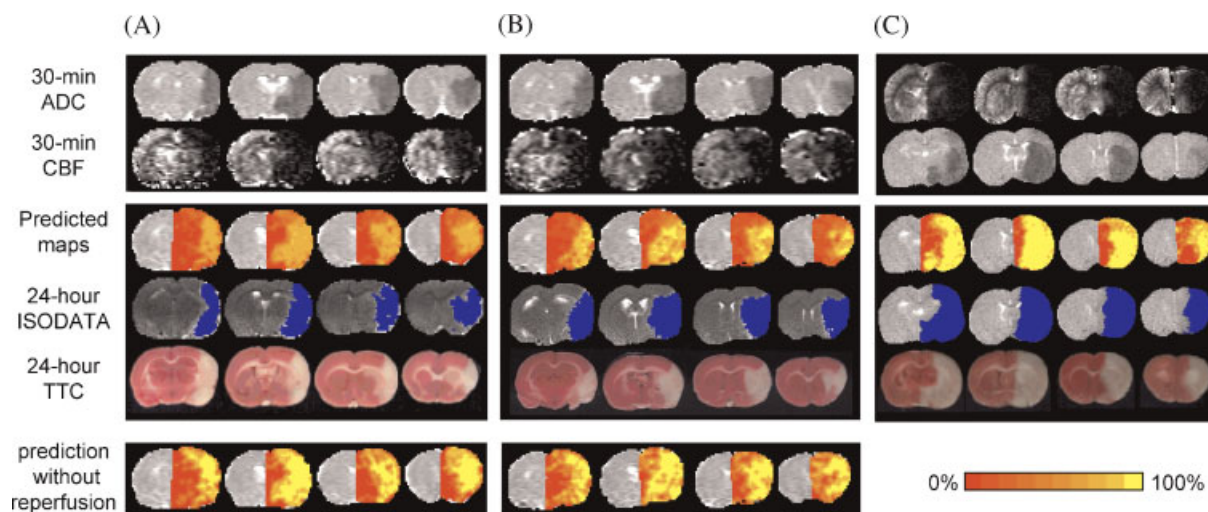


Figure 3. P_1 prediction maps. Predicted infarct maps of risk of subsequent infarction were computed on a separate group of animals for (A) 30-min, (B) 60-min and (C) permanent MCAO based on acute CBF and ADC data. These data are from the experimental groups. Multislice images are posterior to anterior slices from left to right. For comparison, ADC and CBF maps at 30 min, ISODATA analysis of the end-point MRI data, and 2,3,5-triphenyltetrazolium chloride (TTC) histology are also displayed. Predictions made for the hypothetical situation of no reperfusion for the reperfusion groups are also displayed (last row). Color bar = probability of infarct from 0% to 100%. This figure is available in colour online at www.interscience.wiley.com/journal/nbm

and to histological examination. Predictions were also made for the hypothetical situation of no reperfusion for the reperfusion group (Fig. 3, bottom row) by looking up the P_1 contour plots of the permanent MCAO group; higher P_1 and larger areas of infarct were observed in this hypothetical situation, as expected.

ROC analysis was used to quantify prediction accuracy (Fig. 4, experimental dataset). The group-average optimal operating points for the 30-min, 60-min and permanent MCAO groups were, respectively, $47 \pm 5\%$, $43 \pm 12\%$, and

$69 \pm 9\%$, the sensitivities were $82 \pm 6\%$, $82 \pm 7\%$, and $86 \pm 4\%$, the specificities were $83 \pm 5\%$, $86 \pm 5\%$, and $89 \pm 6\%$, and the areas under the ROC curves were $87 \pm 3\%$, $90 \pm 4\%$, and $93 \pm 3\%$. These performance measures indicated reasonably accurate predictions, with predictions made for the permanent MCAO group being most accurate followed by predictions made for the 60-min and 30-min MCAO groups, as expected.

Regional susceptibility to infarction

To improve prediction accuracy, spatial frequency-of-infarct maps were derived (Fig. 5). Spatial frequency-of-infarct and the extent of infarction were heterogeneous. Predictions were made by taking the weighted average of the P_1 map and spatial frequency-of-infarct map. To derive the optimal weighting coefficients, ROC analysis of the prediction accuracy was performed as a function of the weighting coefficients for regional susceptibility information (Fig. 6). The optimal coefficients of spatial frequency-of-infarct were 10% for the permanent MCAO group and, surprisingly, 40% for both the 30-min MCAO and 60-min MCAO groups, indicating that contributions of regional susceptibility information were significant for the reperfusion groups. Figure 7 shows the P_1 maps predicted by using the optimal weighting coefficient of regional susceptibility information. Regional differences between predictions made with and without regional susceptibility information were most apparent in the reperfusion groups, specifically in the cortical tissues close to the anterior communicating artery and caudate tissues near the midline. Importantly, predictions made

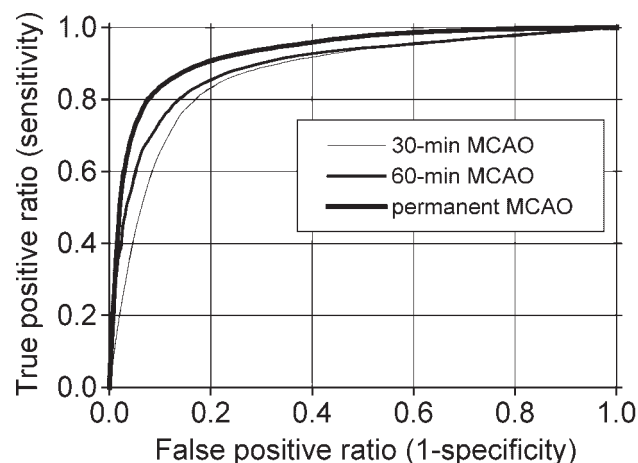


Figure 4. Performance measure of prediction accuracy. ROC curves of sensitivity versus (1 – specificity) of the overall prediction of tissue fate for three different occlusion durations: 30-min MCAO ($n=6$), 60-min MCAO ($n=6$) and permanent MCAO ($n=6$). These data are from the experimental groups. Standard deviation error bars are smaller than 0.05 and are not displayed for clarity.

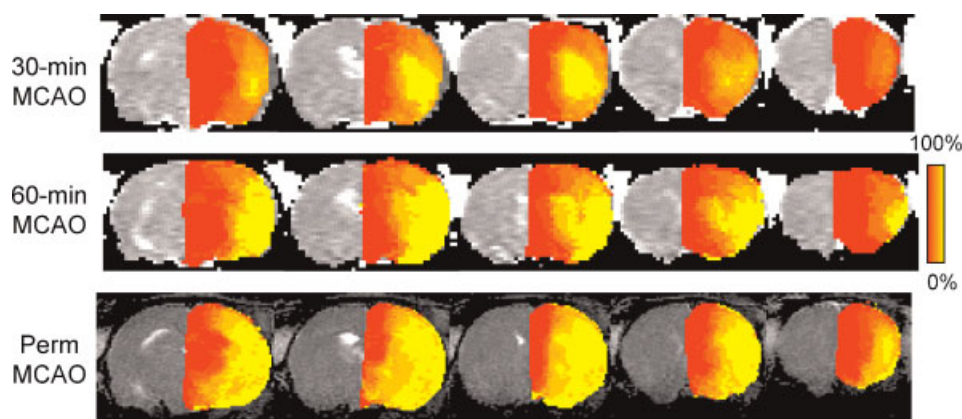


Figure 5. Spatial frequency-of-infarct maps for three different occlusion durations: 30-min, 60-min and permanent MCAO. Color bar = P_1 from 0% to 100%. Displayed images are multislice from caudal to rostral (left to right). This figure is available in colour online at www.interscience.wiley.com/journal/nbm

with regional susceptibility information consistently corresponded better to end-point imaging and histological examination than those made without regional susceptibility information.

DISCUSSION

This study documents the P_1 profiles for three representative MCAO groups in a rat stroke model. Predictions, made on the basis of acute stroke data in the form of P_1 maps, show the likelihood of future infarction on a pixel-by-pixel basis. Performance measures indicate quantitatively accurate predictions. Predictions of infarct made on a hypothetical scenario of non-reperfusion in the reperfusion groups further demonstrate the potential clinical utility of this approach. Moreover, accounting for regional susceptibility to ischemic injury significantly improves prediction accuracy, whereas ADC and CBF data alone, although critical, appeared to be insufficient to accurately predict ischemic tissue fate in stroke with reperfusion. These results could have strong clinical applications and implications.

Statistical predictions based on acute stroke data are sparse. Wu *et al.* (13,35) report the eloquent use of a generalized linear model to predict stroke outcomes based on diffusion-weighted imaging, perfusion-weighted imaging, and T_2 data in humans and rats without 'spatial information.' The sensitivity and specificity of the rat studies of Wu *et al.* (13) are comparable to those in this study.

For the permanent MCAO group, the optimal weighting coefficient for 'spatial information' was 10%, which acts as minor 'spatial smoothing' and thus improves prediction results. However, we were surprised by the large optimal weighting coefficients for 'spatial information' for the reperfusion groups, suggesting that regional susceptibility information played a critical role in accurate prediction of reperfusion stroke. The optimal weighting coefficients were not significantly different between the 30-min and 60-min MCAO groups. One possible explanation is that the sensitivity was not sufficient to detect a difference. Another possible explanation is that the two reperfusion groups had similar amounts of tissue that were susceptible to ischemic injury but in different brain regions. Further investigations are needed. In human stroke, reperfusion is a common

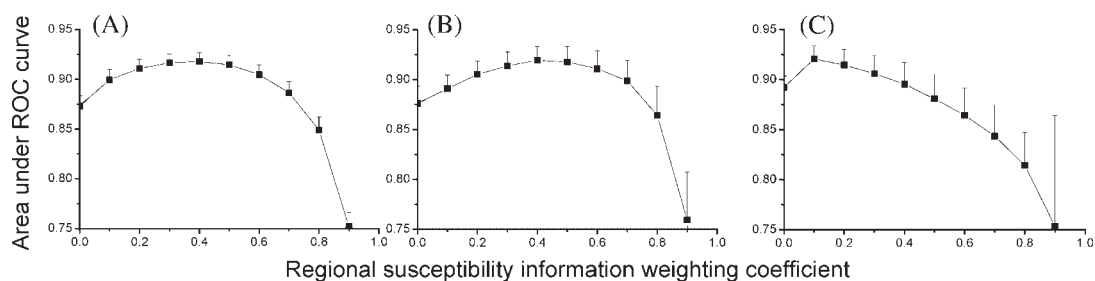


Figure 6. Optimal weighting coefficients of regional susceptibility information. Areas under ROC curves are plotted as a function of regional susceptibility information weighting coefficients. The area under the ROC curves peaks at 0.1 for permanent MCAO and 0.4 for 30-min and 60-min MCAO.

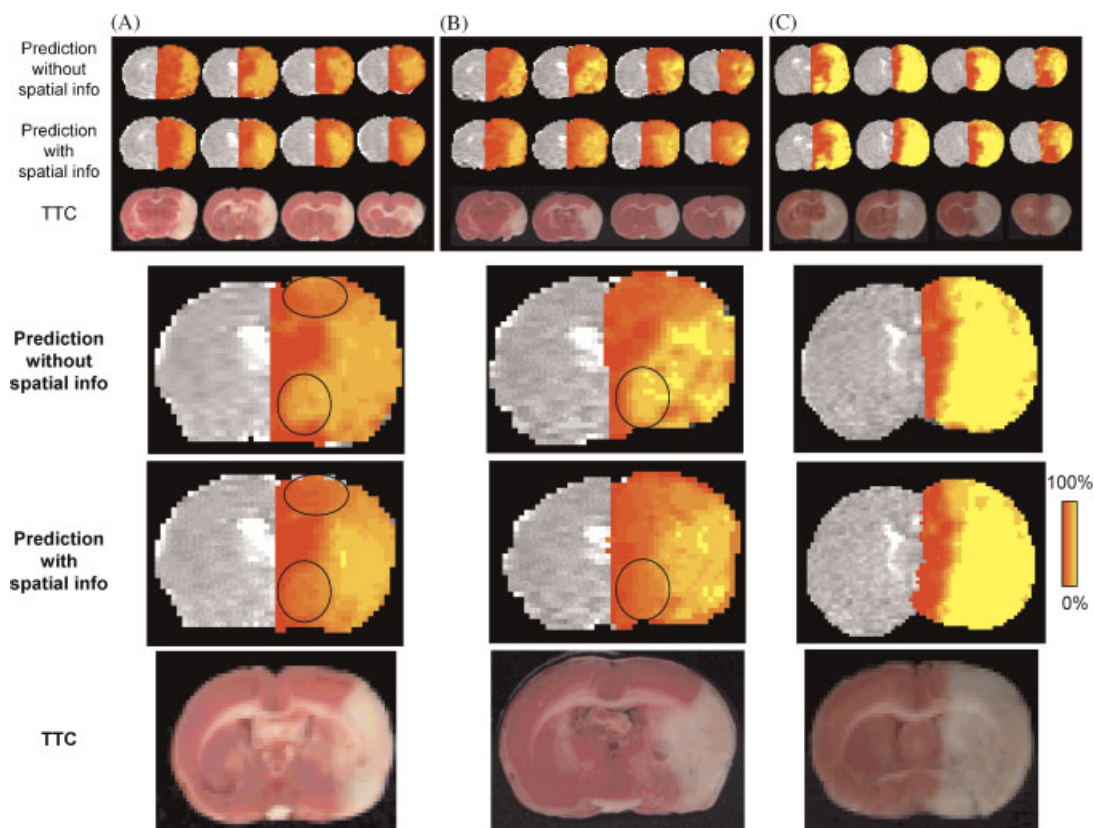


Figure 7. Predictions with and without information on regional susceptibility to infarction (spatial info). P_1 prediction maps with and without regional susceptibility information for three different occlusion durations: 30-min, 60-min and permanent MCAO. The optimal weighting coefficients for regional susceptibility information were used. Histological slides [2,3,5-triphenyltetrazolium chloride (TTC)] are shown for comparison. Displayed images are multislice from caudal to rostral (left to right).

phenomenon, and thus incorporating regional susceptibility information is expected to be more important although less trivial because of increased complexity and heterogeneity. We also expect that the optimal weighting coefficient for ‘spatial information’ in human stroke with reperfusion would be larger because human stroke is more heterogeneous.

Predictions of tissue fate were accurate despite the small sample sizes. The sample sizes of the training basis sets can be readily increased to improve prediction accuracy in a computationally inexpensive manner. Careful categorization of training datasets (i.e. permanent and transient ischemia with or without therapeutic intervention) is important. Establishing proper training basis sets and selecting the proper algorithm in clinical practice is, however, expected to be challenging. Prediction of human stroke requires segmentation of gray and white matter [white matter can be ignored in rats (12)] as they have different susceptibility to infarction. Although P_1 profiles were studied at different time points after stroke, temporal information was not used in predicting tissue fate. The ability to incorporate temporal information to predict ischemic tissue fate is important in clinical settings because stroke patients come into the

emergency room with different stroke onsets which may not be known precisely. Temporal information can be readily incorporated into our predictive model and should be tested first in animal stroke models. Finally, we expect that incorporation of additional information such as pH (36), functional MRI (21,37), vascular permeability (38), oxygen consumption, oxygen extraction fraction (39), sodium MRI, and/or relaxation time (28–31) measurements in stroke will improve prediction accuracy.

This predictive approach could also be applied to other types of brain injury, such as transient ischemic attack and traumatic brain injury. For example, many patients with transient ischemic attack often return to the emergency room with fully developed stroke within 48 h (40). Thus, the ability to predict and identify patients at risk of subsequent stroke should have clinical impact. Translating the success of basic therapeutic research and rodent stroke models into proven interventions in humans has been challenging for many reasons. The heterogeneity of ischemic stroke in humans and the imprecise clinical outcome measures are certainly contributing factors. Accurate and objective prediction models of tissue fate may provide a quantitative framework in decision-making and may help drug trials by accelerating the

identification of promising potential therapies. Finally, this predictive approach could help to individualize the treatment window for stroke patients and extend current treatment window options. Although translating this approach to human applications may not be easy because of the heterogeneity of human ischemic stroke, a similar predictive approach for the study of human stroke has already been reported (11).

In summary, this study establishes a predictive model and incorporates quantitative information about regional susceptibility to infarction to improve the accuracy of predicting the fate of ischemic tissue. This approach may have potential clinical applications in that it could provide quantitative frameworks to aid clinical decision-making in the treatment of acute stroke, to test treatments, and to tailor treatment options for individual patients with acute stroke.

Acknowledgements

This work was supported by the NIH (R01-NS45879) and American Heart Association (SDG-0430020N and SDG-0830293N).

REFERENCES

- Astrup J, Sorensen PM, Sorensen HR. Oxygen and glucose consumption related to Na^+/K^+ transport in canine brain. *Stroke* 1981; **12**: 726–730.
- Hossmann K-A. Viability thresholds and the penumbra of focal ischemia. *Ann Neurol* 1994; **36**: 557–565.
- Lo EH, Moskowitz MA, Jacobs TP. Exciting, radical suicidal: how brain cell die after stroke. *Stroke* 2005; **36**: 189–192.
- Astrup J, Symon L, Siesjö BK. Thresholds in cerebral ischemia: the ischemic penumbra. *Stroke* 1981; **12**: 723–725.
- Moseley ME, Cohen Y, Mintorovitch J, Chileuitt L, Shimizu H, Kucharczyk J, Wendland MF, Weinstein PR. Early detection of regional cerebral ischemia in cats: comparison of diffusion- and T_2 -weighted MRI and spectroscopy. *Magn Reson Med* 1990; **14**: 330–346.
- Warach S. Measurement of the ischemic penumbra with MRI: it's about time. *Stroke* 2003; **34**: 2533–2534.
- Kidwell CS, Alger JR, Saver JL. Beyond mismatch: evolving paradigms in imaging the ischemic penumbra with multimodal magnetic resonance imaging. *Stroke* 2003; **34**: 2729–2735.
- NINDS. Tissue plasminogen activator for acute ischemic stroke. The National Institute of Neurological Disorder, and Stroke rt-PA Stroke Study Group. *N. Engl J Med* 1995; **333**: 1581–1587.
- Arenillas JF, Rovira A, Molina CA, Grive E, Montaner J, Alvarez-Sabin J. Prediction of early neurological deterioration using diffusion- and perfusion-weighted imaging in hyperacute middle cerebral artery ischemic stroke. *Stroke* 2002; **33**: 2197–2203.
- Thomalla GJ, Kucinski T, Schoder V, Fiehler J, Knab R, Zeumer H, Weiller C, Rother J. Prediction of malignant middle cerebral artery infarction by early perfusion- and diffusion-weighted magnetic resonance imaging. *Stroke* 2003; **34**: 1892–1900.
- Wu O, Koroshetz WJ, Ostergard L, Buonanno FS, Copen W, Gonzales G, Rordorf G, Rosen BR, Schwamm LH, Weisskoff RM, Sorensen AG. Predicting tissue outcome in acute human cerebral ischemia using combined diffusion- and perfusion-weighted MR imaging. *Stroke* 2001; **32**: 933–942.
- Shen Q, Ren H, Fisher M, Duong TQ. Statistical prediction of tissue fates in acute ischemic brain injury. *J. Cereb Blood Flow and Metab* 2005; **25**: 1336–1345.
- Wu O, Sumii T, Asahi M, Sasamata M, Ostergaard L, Rosen BR, Lo EH, Dijkhuizen RM. Infarct prediction and treatment assessment with MRI-based algorithms in experimental stroke models. *J. Cereb Blood Flow and Metab* 2007; **27**: 196–204.
- Sobesky J, Zaro Weber O, Lehnhardt FG, Hesselmann V, Neveling M, Jacobs A, Heiss WD. Does the mismatch match the penumbra? Magnetic resonance imaging and positron emission tomography in early ischemic stroke. *Stroke* 2005; **36**: 980–985.
- Guadagno JV, Warburton EA, Jones PS, Fryer TD, Day DJ, Gillard JH, Carpenter TA, Aigbirhio FI, Price CJ, Baron JC. The diffusion-weighted lesion in acute stroke: heterogeneous patterns of flow/metabolism uncoupling as assessed by quantitative positron emission tomography. *Cerebrovasc Dis* 2005; **19**: 239–246.
- Shen Q, Ren H, Bouley J, Fisher M, Duong TQ. Dynamic tracking of acute ischemic tissue fates using improved unsupervised ISODATA analysis of high-resolution quantitative perfusion and diffusion data. *J. Cereb Blood Flow Metab* 2004; **24**: 887–897.
- Smith M-L, Auer RN, Siesjö BK. The density and distribution of ischemic brain injury in the rat following 2–10 min of forebrain ischemia. *Acta Neuropathol* 1984; **64**: 319–332.
- Shen Q, Meng X, Fisher M, Sotak CH, Duong TQ. Pixel-by-pixel spatiotemporal progression of focal ischemia derived using quantitative perfusion and diffusion imaging. *J. Cereb Blood Flow and Metab* 2003; **23**: 1479–1488.
- Shen Q, Fisher M, Sotak CH, Duong TQ. Effects of reperfusion on ADC and CBF pixel-by-pixel dynamics in stroke: characterizing tissue fates using quantitative diffusion and perfusion imaging. *J. Cereb Blood Flow Metab* 2004; **24**: 280–290.
- Meng X, Fisher M, Shen Q, Sotak CH, Duong TQ. Characterizing the diffusion/perfusion mismatch in experimental focal cerebral ischemia. *Ann Neurol* 2004; **55**: 207–212.
- Shen Q, Ren H, Cheng H, Fisher M, Duong TQ. Functional, perfusion and diffusion MRI of acute focal ischemic brain injury. *J. Cereb Blood Flow Metab* 2005; **25**: 1265–1279.
- Duong TQ, Silva AC, Lee S-P, Kim S-G. Functional MRI of calcium-dependent synaptic activity: cross correlation with CBF and BOLD measurements. *Magn Reson Med* 2000; **43**: 383–392.
- Liu ZM, Schmidt KF, Sicard KM, Duong TQ. Imaging oxygen consumption in forepaw somatosensory stimulation in rats under isoflurane anesthesia. *Magn Reson Med* 2004; **52**: 277–285.
- Schmidt KF, Febo M, Shen Q, Ferris CF, Stein E, Duong TQ. Hemodynamic and metabolic changes induced by cocaine in anesthetized rat observed with multimodal functional. *Psychopharmacology* 2006; **185**: 479–486.
- Herscovitch P, Raichle ME. What is the correct value for the brain-blood partition coefficient for water? *J Cereb Blood Flow Metab* 1985; **5**: 65–69.
- Williams DS, Detre JA, Leigh JS, Koretsky AP. Magnetic resonance imaging of perfusion using spin inversion of arterial water. *Proc Natl Acad Sci USA* 1992; **89**: 212–216.
- Wintermark M, Sesay M, Barbier E, Borbely K, Dillon WP, Eastwood JD, Glenn TC, Grandin CB, Pedraza S, Soustiel JF, Nariai T, Zaharchuk G, Caille JM, Dousset V, Yonas H. Comparative overview of brain perfusion imaging techniques. *J. Neuroradiol* 2005; **32**: 294–314.
- Lythgoe MF, Thomas DL, Calamante F, Pell GS, King MD, Busza AL, Sotak CH, Williams SR, Ordidge RJ, Gadian DG. Acute changes in MRI diffusion, perfusion, $\text{T}(1)$, and $\text{T}(2)$ in a rat model of oligemia produced by partial occlusion of the middle cerebral artery. *Magn Reson Med* 2000; **44**: 706–712.
- Kettunen MI, Grohn OH, Lukkarinen JA, Vainio P, Silvennoinen MJ, Kauppinen RA. Interrelations of $\text{T}(1)$ and diffusion of water in acute cerebral ischemia of the rat. *Magn Reson Med* 2000; **44**: 833–839.
- Barbier EL, Liu L, Grillon E, Payen JF, Lebas JF, Segebarth C, Remy C. Focal brain ischemia in rat: acute changes in brain tissue T_1 reflect acute increase in brain tissue water content. *NMR Biomed* 2005; **18**: 499–506.
- Grohn OH MH, Lukkarinen JA, DelaBarre L, Lin J, Garwood M, Kauppinen RA. On- and off-resonance $\text{T}(1\rho)$ MRI in acute cerebral ischemia of the rat. *Magn Reson Med* 2003; **49**: 172–176.

32. Ball GH, Hall DJ. *ISODATA: a novel method of data analysis and pattern classification*. Menlo Park, CA, Stanford Research Institute: 1965.
33. Jacobs MA, Zhang ZG, Knight RA, Soltanian-Zadeh H, Goussev AV, Peck DJ, Chopp M. A model for multiparametric MRI tissue characterization in experimental cerebral ischemia with histological validation in rat: part 1. *Stroke* 2001; **32**: 943–949.
34. Mitsias PD, Jacobs MA, Hammound R, Pasnoor M, Santhakumar S, Papamitsakis NIH, Soltanian-Zadeh H, Lu M, Chopp M, Patel SC. Multiparametric MRI ISODATA ischemic lesion analysis correlation with the clinical neurological deficit and single-parameter MRI techniques. *Stroke* 2002; **33**: 2839–2844.
35. Wu O, Koroshetz WJ, Ostergard L, Buonanno FS, Copen W, Gonzales R, Rordorf G, Rosen BR, Schwamm LH, Weisskoff RM, Sorensen AG. Predicting tissue outcome in acute human cerebral ischemia using combined diffusion- and perfusion-weighted MR imaging. *Stroke* 2001; **32**: 933–942.
36. Zhou J, Payen JF, Wilson DA, Traystman RJ, van Zijl PC. Using the amide proton signals of intracellular proteins and peptides to detect pH effects in MRI. *Nat Med* 2003; **9**: 1085–1090.
37. Dijkhuizen RM, Singhal AB, Mandeville JB, Wu O, Halpern EF, Finklestein SP, Rosen BR, Lo EH. Correlation between brain reorganization, ischemic damage, and neurologic status after transient focal cerebral ischemia in rats: a functional magnetic resonance imaging study. *J. Neurosci* 2003; **23**: 510–517.
38. Dijkhuizen RM, Asahi M, Wu O, Rosen BR, Lo EH. Rapid breakdown of microvascular barriers and subsequent hemorrhagic transformation after delayed recombinant tissue plasminogen activator treatment in a rat embolic stroke model. *Stroke* 2002; **33**: 2100–2104.
39. An H, Lin W. Quantitative measurements of cerebral blood oxygen saturation using magnetic resonance imaging. *J. Cereb Blood Flow Metab* 2000; **20**: 1225–1236.
40. Rothwell PM, Warlow CP. Timing of transient ischemic attacks preceding ischemic stroke. *Neurology* 2005; **64**: 817–820.